Talanta 112 (2013) 111–116

Contents lists available at SciVerse ScienceDirect

Talanta

journal homepage: www.elsevier.com/locate/talanta

Synthesis of PtAu bimetallic nanoparticles on graphene–carbon nanotube hybrid nanomaterials for nonenzymatic hydrogen peroxide sensor

Daban Lu, Yan Zhang, Shaoxiong Lin, Letao Wang, Chunming Wang*

College of Chemistry and Chemical Engineering, Lanzhou University, Lanzhou 730000, PR China

ARTICLE INFO

Article history:
Received 13 November 2012
Received in revised form
3 March 2013
Accepted 5 March 2013
Available online 13 March 2013

Keywords:
PtAu bimetallic nanoparticles
Graphene
Multi walled carbon nanotubes
Nonenzymatic
Hydrogen peroxide sensor

ABSTRACT

PtAu bimetallic nanoparticles (NPs) were successfully synthesized on graphene sheets-multi walled carbon nanotubes (G-CNTs) hybrid nanomaterials via a simple one-step chemical co-reduction method in ethylene glycol (EG)–water system. The nanocomposites (PtAu/G-CNTs) were characterized by X-ray diffraction (XRD), transmission electron microscopy (TEM) and X-ray photoelectron spectroscopy (XPS). Then a sensitive nonenzymatic hydrogen peroxide (H_2O_2) sensor was fabricated based on PtAu/G-CNTs nanocomposites modified glassy carbon electrode (GCE). The results of electrochemical experiments demonstrated that the sensor exhibited excellent electrocatalytic activity to the reduction of H_2O_2. The sensor displayed a fast amperometric response time of less than 4 s with linear detection range from 2.0 to 8561 μM and a relatively low detection limit of 0.6 μM ($S/N=3$). In addition, the sensor also showed good selectivity for H_2O_2 detection, long-term stability and reproducibility.

1. Introduction

Hydrogen peroxide (H_2O_2) plays a significant role in many areas including clinic, food control, pharmaceutical and environmental protection [1,2]. Therefore, many analytical methods have been developed for the detection of H_2O_2, such as fluorescence [3], spectrophotometry [4], chemiluminescence [5] and electrochemistry methods [6–8]. Among these analytical techniques, electrochemical detection of H_2O_2 is distinctive for its high sensitivity, selectivity and simplicity. Enzyme and nonenzymatic based electrochemical sensors have been extensively employed in H_2O_2 determination [9,10]. However, the enzyme-modified electrodes display many disadvantages, such as instability, high cost of enzymes and complicated immobilization procedure. Thus, nonenzymatic H_2O_2 sensors based on functional nanocomposites have been developed owing to its high stability, easy handling and wide responding. The development of a high sensitivity and good selectivity catalyst for nonenzymatic H_2O_2 detection is still highly desirable in this field.

Platinum (Pt) nanoparticles (NPs) have attracted much attention for their superior catalysis for many chemical reactions [11]. However, pure Pt catalyst is rather expensive and can be easily poisoned by adsorbed intermediates. Thus, Pt-based bimetallic nanocatalyst has been attracted widespread interests in recent years, which aimed to improve the catalytic activity as well as reduce the cost of catalysts. The aim of our work is to enhance the catalytic properties towards H_2O_2 by investigating more active and lower cost replacements to pure Pt. Moreover, the stability of the Pt catalyst can be significantly improved after the incorporation of Au [12]. Unfortunately, high surface energy of particles with diameters in nanometers may aggregate. Thus, the catalytic activity of the nanoparticles will decrease [13]. In order to improve the catalytic activity, carbonaceous materials, such as mesoporous carbon [14], graphene [15] and carbon nanotubes (CNTs) [16], have generally been employed as the support materials for nanoparticles.

Graphene, a monolayer of carbon atoms closely packed into honeycomb two-dimensional carbon material, has attracted enormous attention from both the experimental and theoretical science communities [17–19]. However, due to van der Waals interactions and strong π–π stacking, graphene sheets tend to form irreversible agglomerates and even restack to form graphite. Thus, both large specific surface area and outstanding single-layer electric property of graphene are sacrificed [20]. The performances of graphene sheets are significantly worse than expected, limiting their further applications. This phenomenon is the most important issue for realizing the applications of graphene sheets to electrode materials. Additionally, graphene sheets prepared through the chemical reduction will leave behind some defects and vacancies [21]. Meanwhile, the conductivity of the graphene sheets will reduce. These problems severely restrict the further applications for the catalyst supports. This can be prevented by using spacers and CNTs can be employed as space impediments [22] between the graphene sheets to prevent the restacking of graphene. Using CNTs as spacers could result in the increase of the surface area, electronic conductivity, additional flexibility and mechanical stability of graphene, and thereby the enhancement in performance. Thus, incorporate the advantages of two-dimensional graphene sheets and one-dimensional CNTs in the

* Corresponding author. Tel.: +86 931 8911895; fax: +86 931 8912582.
E-mail address: wangcm@lzu.edu.cn (C. Wang).

0039-9140/$ - see front matter © 2013 Elsevier B.V. All rights reserved.
http://dx.doi.org/10.1016/j.talanta.2013.03.010

planar and axial directions, the graphene sheets and CNTs hybrid (G-CNTs) as catalyst support materials may increase catalytic activity of nanoparticles. As a result, the CNTs ensure the high electrochemical utilization of graphene sheets.

In this work, PtAu bimetallic NPs were successfully synthesized on G-CNTs hybrid nanomaterials via a simple one-step chemical co-reduction method in ethylene glycol (EG)–water system. Then a nonenzymatic H_2O_2 sensor was fabricated based on PtAu/G-CNTs nanocomposites modified glassy carbon electrode (GCE). The electrochemical results demonstrate that the sensor exhibited superior electrocatalytic activity towards the reduction of H_2O_2. The sensor presents high sensitivity towards the detection of H_2O_2, along with a low detection limit and a wide linear range.

2. Experiments

2.1. Materials and apparatus

Graphite flake (nature, −325 mesh) was from Alfa Aesar (Beijing, China). MWCNTs-COOH was purchased from Shenzhen Nanotech Port Co., Ltd. H_2PtCl_6 and $HAuCl_4$ were purchased from Tianjin Chemical Factory (Tianjin, China). H_2O_2 (30%) was obtained from Sinopharm Chemical Reagent Co., Ltd. 0.1 M phosphate buffer solution (PBS, pH=7.0) was prepared with 0.1 M Na_2HPO_4 and 0.1 M NaH_2PO_4. All other reagents and solvents were of analytical grade and used without further purification. All chemicals were prepared with deionized water purified via Milli-Q unit.

Electrochemical measurements were performed on a CHI 832 electrochemical workstation (CH Instrument, China) with a three-electrode system consisting of a platinum wire auxiliary, an saturated calomel electrode (SCE) reference and a bare or modified GCE (Φ=3 mm) working electrode. The phase structures of the samples were determined by X-ray diffraction (XRD) using a D/Max 2400 Rigaku diffractometer with Cu-K_α radiation (k=0.15418 nm). The morphology of the samples was characterized using high resolution transmission electron microscopy (HRTEM, Tecnai G^2 F30, FEI, USA). X-ray photoelectron spectroscopy (XPS) was performed on a VG ESCA LAB 210 electron spectrometer using an Mg-K_α line excitation source with the reference of C1s at 285.0 eV.

2.2. Synthesis of PtAu/G-CNTs nanocomposites

Graphene oxide (GO) was prepared from graphite by a modified Hummers method [23]. The PtAu/G-CNTs nanocomposite materials were prepared by a chemical co-reduction of Pt and Au precursor salts in ethylene glycol (EG)–water solutions as shown in Fig. 1. Briefly, GO (30 mg) and MWCNTs-COOH (10 mg) were added into deionized water (8.14 mL), and then the mixture was ultrasonically treated for 2 h to form a stable dispersion. Sequentially, 0.0193 M H_2PtCl_6 solution (1.04 mL), 0.0243 M $HAuCl_4$ solution (0.82 mL) and EG (40 mL) was injected into the mixture and ultrasonically treated for another 1 h, then the mixture was kept at 120 °C for 24 h under magnetic stirring. The resulting nanocomposites were collected by filtration and washed copiously with deionized water for several times, and then dried in vacuum. The G-CNTs, Au/G-CNTs, Pt/G-CNTs, PtAu/CNTs and PtAu/G catalysts were achieved through the same procedures.

2.3. Fabrication of electrochemical sensor

Before modification, the bare GCE was polished to a mirror-like surface with 0.3 and 0.05 μm alumina slurry, and cleaned ultrasonically in deionized water for 2 min. Subsequently, the electrode was sonicated in nitric acid (1:1 volume ratio), and then in absolute ethanol. Finally, it was cleaned ultrasonically in deionized water.

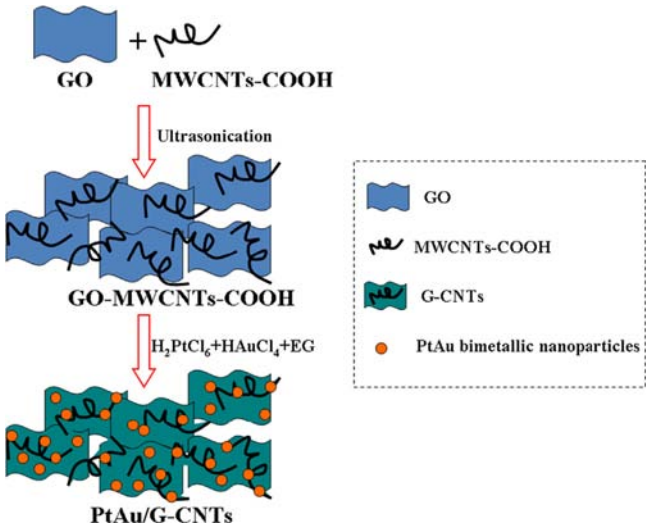

Fig. 1. Schematic representation for the synthesis of PtAu/G-CNTs nanocomposites.

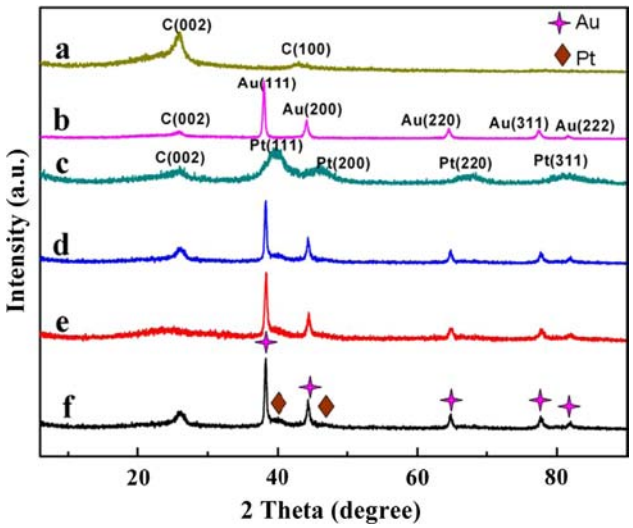

Fig. 2. XRD patterns of (a) G-CNTs, (b) Au/G-CNTs, (c) Pt/G-CNTs, (d) PtAu/CNTs, (e) PtAu/G and (f) PtAu/G-CNTs.

PtAu/G-CNTs nanocomposite (1.0 mg mL^{-1}) dimethylformamide solution was obtained by ultrasonication for 2 h to form a homogeneous mixture. Then, 5 μL of the mixture was dropped on the pretreated GCE and dried in a desiccator. For comparison, the other modified electrodes were prepared with the similar procedure. The electrolyte solutions were deoxygenated with N_2 for 30 min and kept under N_2 atmosphere during electrochemical examinations.

3. Result and discussion

3.1. Characterization of the PtAu/G-CNTs nanocomposites

The XRD patterns of G-CNTs, Au/G-CNTs, Pt/G-CNTs, PtAu/CNTs, PtAu/G and PtAu/G-CNTs are shown in Fig. 2. The XRD pattern of the G-CNTs (curve *a*) exhibits intense peaks at 2θ about 26° corresponding to the C (002) plane. This peak is common to both graphene and CNTs [24]. The diffraction peak at around 43° is associated with the (100) plane of the hexagonal structure of carbon. The XRD of the G-CNTs hybrid nanomaterials is the first confirmation of reduction of GO, as it does not have a peak at 10.6°. The broadness of the XRD intensities indicates that nanometre-sized crystallites were formed in the hybrid nanomaterials [24].

The diffraction patterns for Au/G-CNTs (curve *b*) and Pt/G-CNTs (curve *c*) show a face-centered-cubic (fcc) structural characterization. The 2θ value of (111) peak for Au/G-CNTs is seen at 38.1° and that for Pt/G-CNTs at 39.86°. Taking into account that the nominal composition (Pt:Au) is 1:1 in the Pt and Au precursor salts, the (111) reflection of the nanocomposites should appear in between Au/G-CNTs (38.1°) and Pt/G-CNTs (39.86°) for alloy conformation. By contrast, the nanocomposites, (d) PtAu/CNTs, (e) PtAu/G and (f) PtAu/G-CNTs, show two sets of such reflections. This is not in agreement with the alloy reflections [25]. This clearly indicates the dominant bimetallic nature of the nanocomposite as the reflections observed for Au (38.28°) and Pt (39.84°) in PtAu/G-CNTs are very close to that observed for individual monometallic Au/G-CNTs (38.1°) and Pt/G-CNTs (39.86°). Similar behaviour was observed for all other bimetallic compositions. This indicates condensation of two different crystalline phases although both correspond to the same crystalline structure type [26]. Merger of the peaks between 38.1° (Au) and 39.86° (Pt) further indicates that the nanoparticles are bimetallic in nature, as observed by other reports [27–29].

The morphologies of G-CNTs, PtAu/CNTs, PtAu/G and PtAu/G-CNTs were characterized by TEM. As shown in Fig. 3A, the graphene sheets and the CNTs formed uniform hybrid nanomaterials with the CNTs absorbed on the surface of the graphene sheets or filled between the graphene sheets. From the images in Fig. 3B and C, the PtAu bimetallic NPs are slightly more uniformly dispersed on the graphene sheets than the CNTs. These results might be attributed to the remained oxygen-containing functionalities on the surface of the graphene sheets [30]. As shown in Fig. 3D, the G-CNTs supports are decorated by the nanosized PtAu bimetallic NPs with very few aggregations and no particles scattered out of the support, indicating a strong interaction between the G-CNTs supports and particles. Additionally, by functioning as spacers, these CNTs attached onto the graphene sheets surface can prevent the reduced graphene sheets from aggregation and restacking. Both the faces of graphene sheets are accessible in their applications. Therefore, the G-CNTs supports possess large surface areas, and nanoparticles can be deposited on both sides of these supports. Highly dispersed PtAu bimetallic NPs on G-CNTs supports with larger surface areas has advantages in catalytic activity and sensor sensitivity [31]. Furthermore, the CNTs in the hybrid nanomaterials set up a fairly conductive network, which may facile charge-transfer and mass-transfer processes. Thus, the PtAu/G-CNTs may have good performance in catalysis. In addition, the composition of PtAu bimetallic NPs analyzed by energy-dispersive X-ray spectroscopy (EDX) (Fig. 3E). It has an elemental composition of 45.9 at% Pt and 54.1 at% Au, which is consistent with the Pt:Au ratio in the precursor (with platinum to gold mole ratio of 1:1). The histogram of particle size distribution (Fig. 3F) shows that PtAu bimetallic NPs on G-CNTs have a narrow size distribution and the average diameter was about 3.6 nm. Obviously, chemical reduction method usually results in smaller sizes of nanoparticles than electrochemical deposition, which is helpful to enhance the catalytic activity and sensor sensitivity [32].

In addition, we employed the XPS measurements to further determine the chemical composition of the PtAu/G-CNTs nanocomposites. The C1s spectrum shows peaks at 284.4, 285.8, and 288.2 eV, which correspond to C–C, C–OH, and O–C=O chemical binding states, respectively (Fig. 4A). These observations indicated that GO was not completely reduced with a spot of oxygen-containing functional groups during reduction process. But the intensity of the peaks of the oxygen-containing functional groups was very weak, indicating that the as-prepared G-CNTs hybrid nanomaterials had a high reduction level. As can be seen from the high-resolution XPS spectrum in Fig. 4B, two obvious peaks at 75.0 and 71.8 eV can be easily observed, assigning to the Pt $4f_{5/2}$ and $4f_{7/2}$. The Au 4f high-resolution XPS spectrum is shown in Fig. 4C, the two broad peaks at binding energies of about 87.7 and 84.0 eV were attributed to Au $4f_{5/2}$ and $4f_{7/2}$. From the analysis, we can estimate that the bimetallic nanoparticles were composed of Pt and Au.

3.2. Electrochemical performances of the PtAu/G-CNTs/GCE towards H_2O_2

Fig. 5 shows cyclic voltammetry (CV) responses of 5.0 mM H_2O_2 in 0.1 M N_2-saturated PBS (pH=7.0) at different electrodes.

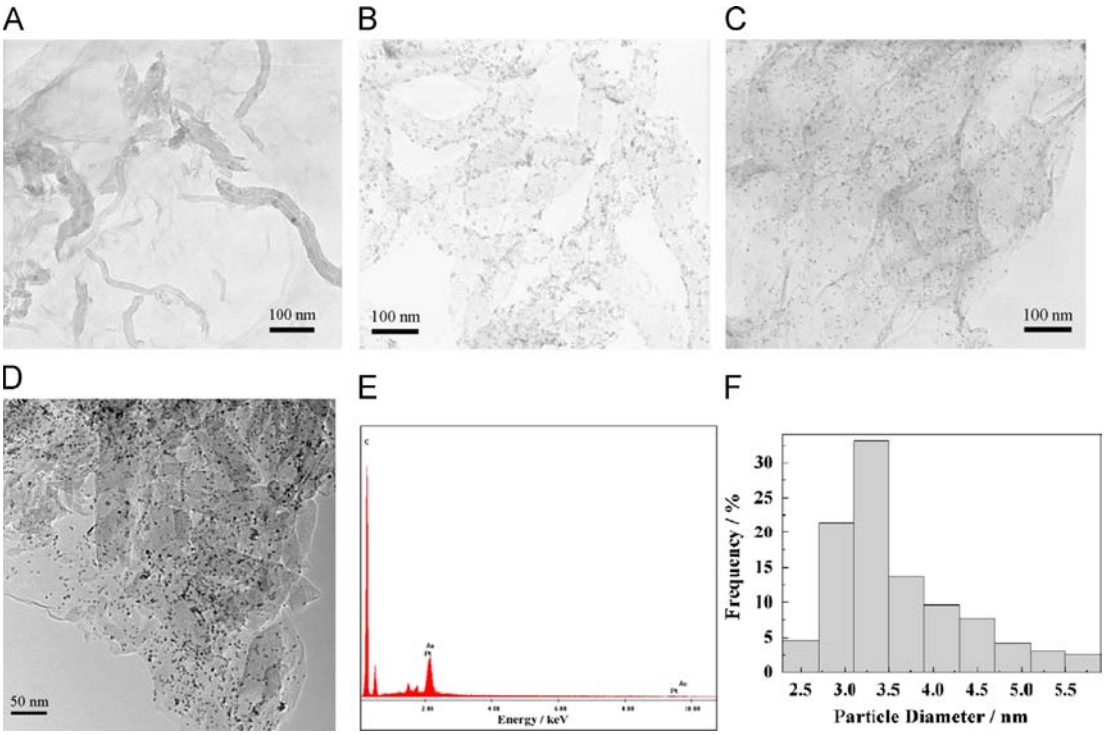

Fig. 3. TEM images of (A) G-CNTs, (B) PtAu/CNTs, (C) PtAu/G, and (D) PtAu/G-CNTs. (E) EDX spectrum of PtAu/G-CNTs. (F) Histogram of particle size distribution.

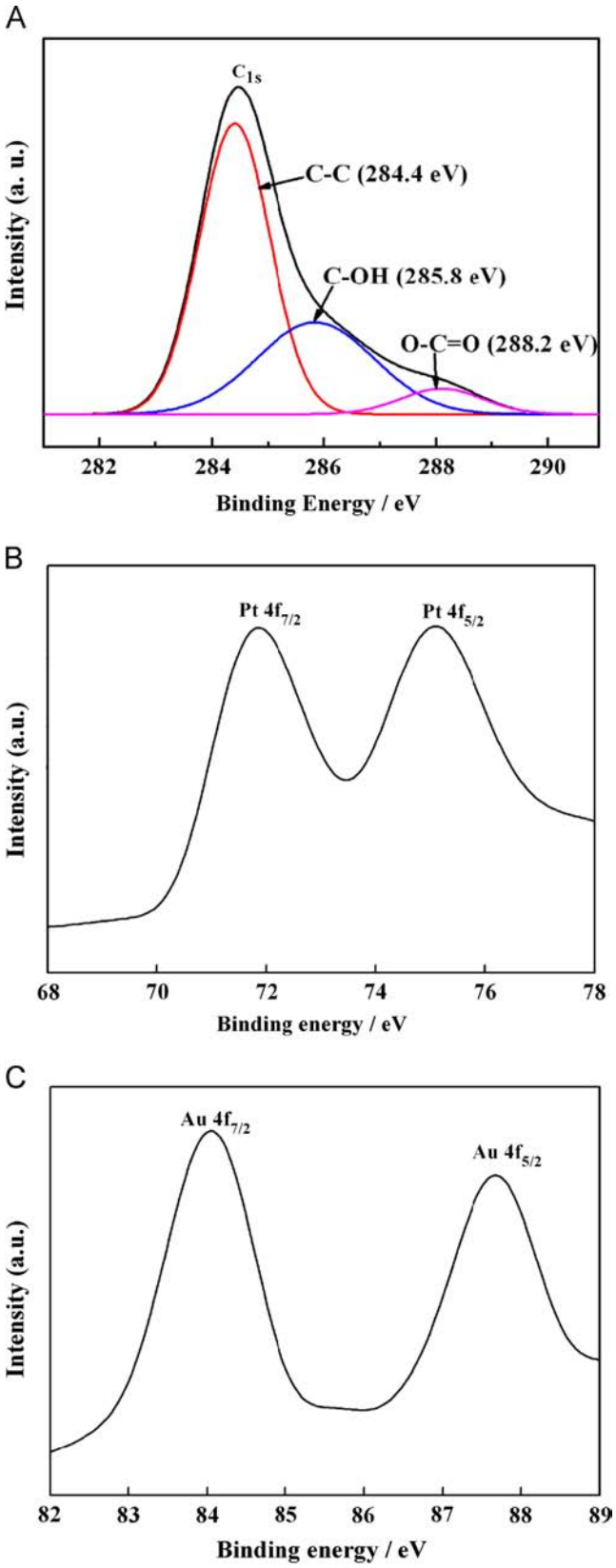

Fig. 4. XPS spectrum of the PtAu/G-CNTs: (A) C1s, (B) Pt 4f, (C) Au 4f.

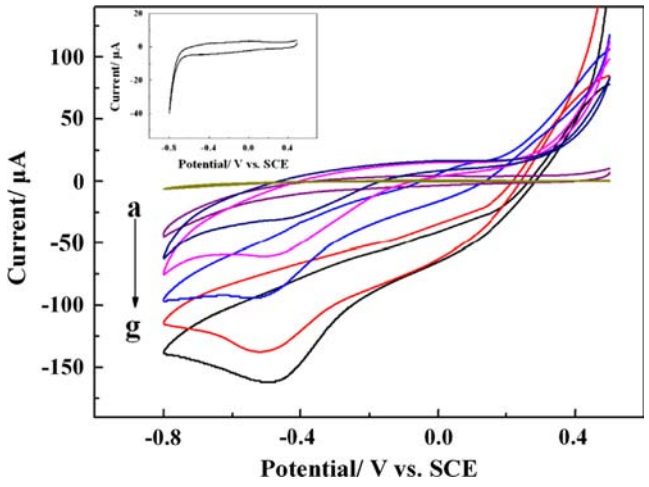

Fig. 5. Cyclic voltammograms of (a) bare GCE, (b) G-CNTs/GCE, (c) Au/G-CNTs/GCE, (d) Pt/G-CNTs/GCE, (e) PtAu/CNTs/GCE, (f) PtAu/G/GCE, and (g) PtAu/G-CNTs/GCE in 0.1 M PBS (pH=7.0) containing 5 mM H_2O_2 at a scan rate of 10 mV s^{-1}. Inset: the Cyclic voltammograms of PtAu/G-CNTs/GCE in 0.1 M PBS (pH=7.0) without H_2O_2.

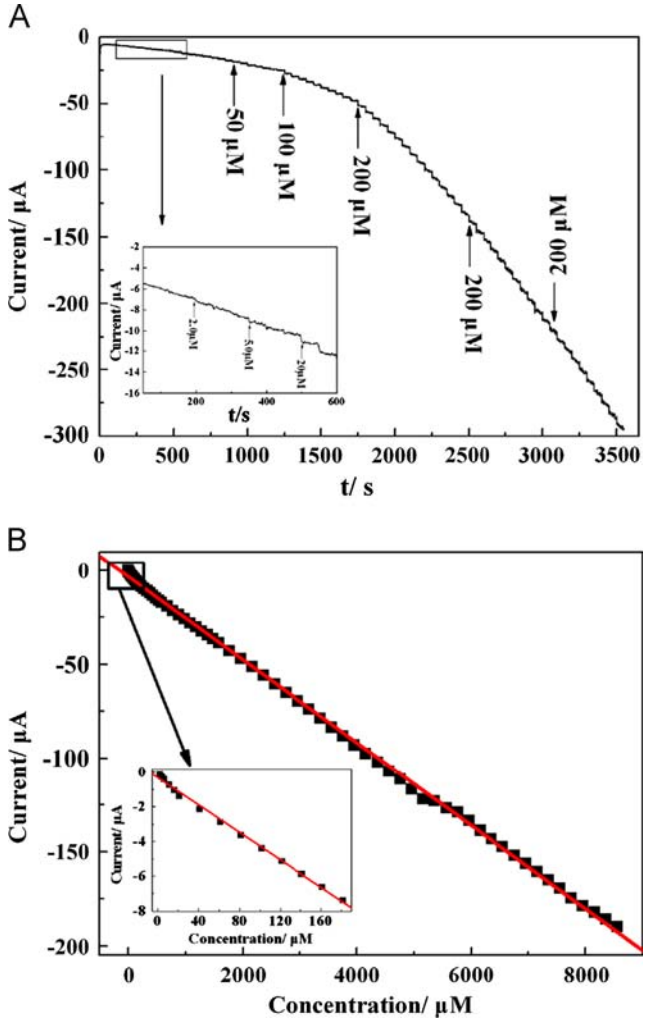

Fig. 6. (A) Current–time response curve for successive injection of H_2O_2 at PtAu/G-CNTs/GCE measured at −0.47 V. Inset: magnified image of the region in the rectangle. (B) Calibration curves of response current versus H_2O_2 concentration at PtAu/G-CNTs/GCE. Inset: magnified image of the region in the rectangle.

No redox peaks are observed in the absence of H_2O_2 for PtAu/G-CNTs/GCE (Inset of Fig. 5), indicating that the modified electrode is non-electroactive in the selected potential region. After 5.0 mM H_2O_2 was added into the N_2-saturated PBS, no reduction peak was observed on bare GCE (curve *a*) and G-CNTs/GCE (curve *b*), which indicated that H_2O_2 reduction could not be achieved at the bare GCE and G-CNTs/GCE. In contrast, the Au/G-CNTs/GCE (curve *c*),

Pt/G-CNTs/GCE (curve *d*), PtAu/CNTs/GCE (curve *e*) and PtAu/G/GCE (curve *f*) all display a prominent reduction peak current around −0.47 V, suggesting that H_2O_2 reduction was realized. As can be seen in curve *g*, the PtAu/G-CNTs/GCE shows the largest reduction peak current compared to the other electrodes. The PtAu/G-CNTs exhibits much better electrocatalytic ability towards H_2O_2. This improved electrocatalytic ability could be attributed to the synergistic effect of PtAu bimetallic NPs and G-CNTs, in which PtAu bimetallic NPs has electrocatalytic ability towards H_2O_2 and the G-CNTs provides a large specific surface area to increase the loading amount of H_2O_2. Enhancement of Pt activity for catalysis by Au NPs is owing to the optimum dispersion of the Pt phase on Au rather than to tuning of the electronic properties of Pt through interaction with the Au NPs [26]. Therefore, the incorporation of Au into Pt improves both electrocatalytic activity and stability. Moreover, Fernández et al. [33] proposed that the superior electrocatalytic activity is attributed to the formation of PtAu bimetallic NPs. Additionally, due to the advantage of the conducting network structure of CNTs, the G-CNTs hybrid has higher surface area, good electronic conductivity, additional flexibility and excellent mechanical stability. In addition, incorporate the advantages of graphene sheets and CNTs in the planar and axial directions, the high surface area of G-CNTs hybrid as a good catalyst support provided large amount of anchoring sites for achieving a high dispersion of PtAu bimetallic NPs during the synthesis of the nanocomposite. Thus, the PtAu bimetallic NPs will not from serious aggregation, and can preserve its high catalytic performance.

3.3. Amperometric response and calibration curve for H_2O_2 detection

Fig. 6A shows typical amperometric response of the PtAu/G-CNTs/GCE with successive additions of H_2O_2 with different concentrations into 0.1 M N_2-saturated PBS (pH 7.0) at an applied potential of −0.47 V. As can be seen, PtAu/G-CNTs/GCE responds quickly to the change of H_2O_2 concentration and can achieve 95% of the maximum steady-state current within 4 s after the addition of H_2O_2, indicating a fast diffusion of the substrate in the hybrid film modified electrode. The corresponding current-concentration calibration curve in Fig. 6B clearly shows that the PtAu/G-CNTs/GCE displays a remarkable sensitivity. The linear response range of the PtAu/G-CNTs/GCE with the concentration of H_2O_2 was from 2.0 to 8561 μM with a detection limit of 0.6 μM based on a signal-to-noise ratio (*S*/*N*) of 3, and the sensitivity was calculated to be 313.4 μA mM^{-1} cm^{-2}. The regression equation is $I(\mu A) = -0.02214CH_2O_2 - 3.231$ with a correlation coefficient of 0.9983. A comparison of linear range and detection limit of our sensor with other H_2O_2 sensors reported previously is shown in Table 1. It can be observed that the performances of our sensor are comparable and even better than those obtained at several electrodes reported recently. This could be contributed to the higher electrocatalytic ability of PtAu bimetallic NPs towards H_2O_2 and the large specific surface area of G-CNTs to increase the loading amount of H_2O_2. Therefore, the PtAu/G-CNTs nanocomposites are good modified electrode materials for preparation of low detection limit and wide linear range amperometric sensor for H_2O_2.

3.4. Interference study

For evaluating selectivity of the PtAu/G-CNTs/GCE, some possible interferents were investigated for their effect on the amperometric detection of H_2O_2. Fig. 7 was the amperometric response obtained by successive additions of 200 μM H_2O_2 and some possible interferents in 0.1 M N_2-saturated PBS (pH 7.0) at an applied potential of −0.47 V. As shown in Fig. 7, the response current of ascorbic acid (AA), dopamine (DA), uric acid (UA), glucose, sucrose and citric acid do not cause any observable interference to the detection of H_2O_2. This suggests that these species had no obvious interference in the reduction of H_2O_2. The selectivity for H_2O_2 amperometric detection is very good on PtAu/G-CNTs/GCE.

3.5. Stability and reproducibility

Furthermore, the fabrication reproducibility of the PtAu/G-CNTs/GCE was also investigated. The relative standard deviation (RSD) of current signal for 200 μM H_2O_2 at six modified electrodes prepared at the same conditions was 4.37%, suggesting the good reproducibility and precision. After the modified electrode was stored in refrigerator at 4 °C for 2 weeks, the current response to 200 μM H_2O_2 remained 93.18% of its original response. The results demonstrate that the sensor exhibits excellent long-term stability.

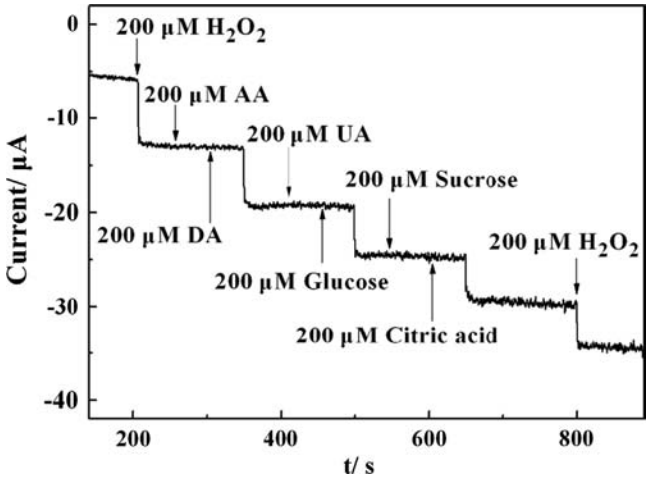

Fig. 7. Current–time response curve of the PtAu/G-CNTs/GCE upon successive addition of 200 μM H_2O_2, AA, DA, UA, glucose, sucrose and citric acid in 0.1 M PBS (pH = 7.0) at −0.47 V.

Table 1
Comparison of the performance of various H_2O_2 sensors.

Electrode materials	Linear range (μM)	Detection limit (μM)	References
Se/Pt nanocomposites	10–15,000	3.1	[8]
Ag NPs/type I collagen networks	5,000–40,600	0.7	[10]
MnO_2/graphene oxide nanocomposite	5–600	0.8	[34]
Ag NP/rGO	100–100,000	31.3	[35]
Fe_3O_4–Ag hybrid submicrosphere	1.2–3,500	1.2	[36]
Pt NPs/ordered mesoporous carbon nanocomposite	2–4,212	1.2	[37]
Pt/Graphene nanocomposites	2.5–6,650	0.8	[38]
Pt/polypyrrole hybrid hollow microspheres	1,000–8,000	1.2	[39]
PtAu/G-CNTs	2–8,561	0.6	This work

4. Conclusions

In this work, PtAu bimetallic NPs were successfully synthesized on G-CNTs hybrid nanomaterials via a simple one-step chemical co-reduction method in EG-water system. The PtAu/G-CNTs modified GCE as a nonenzymatic sensor exhibited a high electrocatalytic activity for the H_2O_2 detection. The electrochemical results showed that the sensor had high sensitivity, good selectivity, with a wide linear range and low detection limit for amperometric detection of H_2O_2. The sensor also exhibited good stability and reproducibility. Therefore, this work provided a promising platform for the study of the high surface area and good conductivity of the G-CNTs hybrid nanomaterials, and the catalytic nature of PtAu bimetallic NPs. The PtAu/G-CNTs might be an effective material for the construction of attractive nonenzymatic amperometric H_2O_2 sensor in the future.

Acknowledgements

This work was supported by the National Natural Science Foundation of China under Grant no. 20775030.

References

[1] J. Wang, Y. Lin, L. Chen, Analyst 118 (1993) 277.
[2] A.A. Karyakin, E.E. Karyakina, L. Gorton, Anal. Chem. 72 (2000) 1720.
[3] Z. Rosenzweig, R. Kopelman, Anal. Chem. 68 (1996) 1408.
[4] C. Matsubara, N. Kawamoto, K. Takamura, Analyst 117 (1992) 1781.
[5] L. Luo, Z. Zhang, Anal. Chim. Acta 580 (2006) 14.
[6] A. Safavi, N. Maleki, E. Farjami, Electroanalysis 21 (2009) 1533.
[7] C.M. Welch, C.E. Banks, A.O. Simm, R.G. Compton, Anal. Bioanal. Chem. 382 (2005) 12.
[8] Y. Li, J.J. Zhang, J. Xuan, L.P. Jiang, J.J. Zhu, Electrochem. Commun. 12 (2010) 777.
[9] K.F. Zhou, Y.H. Zhu, X.L. Yang, J. Luo, C.Z. Li, S.R. Luan, Electrochim. Acta 55 (2010) 3055.
[10] Y.H. Song, K. Cui, L. Wang, S.H. Chen, Nanotechnology 20 (2009) 105501.
[11] B.C.H. Steele, A. Heinzel, Nature 414 (2001) 345.
[12] H. Zhu, Y.L. Liu, L.B. Shen, Y.S. Wei, Z.J. Guo, H.J. Wang, K.F. Han, Z.R. Chang, J. Int., Hydrogen Energy 35 (2010) 3125.
[13] M. Zhao, L. Sun, R.M. Crooks, J. Am. Chem. Soc. 120 (1998) 4877.
[14] F.B. Su, J.H. Zeng, X.Y. Bao, Y.S. Yu, J.Y. Lee, X.S. Zhao, Chem. Mater. 17 (2005) 3960.
[15] Y.J. Li, W. Gao, L.J. Ci, C.M. Wang, P.M. Ajayan, Carbon 48 (2010) 1124.
[16] S.J. Guo, S.J. Dong, E.K. Wang, Adv. Mater. 22 (2010) 1269.
[17] L.A. Ponomarenko, F. Schedin, M.I. Katsnelson, R. Yang, E.W. Hill, K. S. Novoselov, A.K. Geim, Science 320 (2008) 356.
[18] D. Li, R.B. Kaner, Science 320 (2008) 1170.
[19] K.S. Novoselov, A.K. Geim, S.V. Morozov, D. Jiang, M.I. Katsnelson, I. V. Grigorieva, S.V. Dubonos, A.A. Firsov, Nature 438 (2005) 197.
[20] D.B. Lu, S.X. Lin, L.T. Wang, X.Z. Shi, C.M. Wang, Y. Zhang, Electrochim. Acta 85 (2012) 131.
[21] C. Gomez-Navarro, J.C. Meyers, R.S. Sundaram, A. Chuvilin, S. Kurash, M. Burghard, K. Kern, U. Kaizer, Nano Lett. 10 (2010) 1144.
[22] R.I. Jafri, T. Arockiados, N. Rajalakshmi, S. Ramaprabhu, J. Electrochem. Soc. 157 (2010) B874.
[23] W.S. Hummers, R.E. Offeman, J. Am. Chem. Soc. 80 (1958) 1339.
[24] S. Sasikaladevi, J. Aravind, V. Eswaraiah, S Ramaprabhu, J. Mater. Chem. 21 (2011) 15179.
[25] J.B. Xu, T.S. Zhao, Z.X. Liang, J. Power Sources 185 (2008) 857.
[26] S.S. Kumar, K.L.N. Phani, J. Power Sources 187 (2009) 19.
[27] M.L Wu, D.H. Chen, T.C. Huang, Chem. Mater. 13 (2001) 599.
[28] B. Singha, F. Laffirb, T. McCormacc, E. Dempsey, Sens. Actuators, B 150 (2010) 80.
[29] Y.J. Hu, H. Zhang, P. Wu, H. Zhang, B. Zhou, C.X. Cai, Phys. Chem. Chem. Phys. 13 (2011) 4083.
[30] S.D. Yang, C.M. Shen, X.J. Lu, H. Tong, J.J. Zhu, X.G. Zhang, H.J. Gao, Electrochim. Acta 62 (2012) 242.
[31] Y.C. Xing, J. Phys. Chem. B 108 (2004) 19255.
[32] F. Xiao, F.Q. Zhao, L.Z. Deng, B.Z. Zeng, Electrochem. Commun. 12 (2010) 620.
[33] P.H. Fernández, S. Rojas, P. Ocón, A. de Frutos, J.M. Figueroa, P. Terreros, M. A. Peña, J.L.G. Fierro, J. Power Sources 177 (2008) 9.
[34] L.M. Li, Z.F. Du, S. Liu, Q.Y. Hao, Y.G. Wang, Q.H. Li, T.H. Wang, Talanta 82 (2010) 1637.
[35] S. Liu, J.Q. Tian, L. Wang, X.P. Sun, Carbon 49 (2011) 3158.
[36] Z.L. Liu, B. Zhao, Y. Shi, C.L. Guo, H.B. Yang, Z. Li, Talanta 81 (2010) 1650.
[37] X.J. Bo, J.C. Ndamanisha, J. Bai, L.P. Guo, Talanta 82 (2010) 85.
[38] F.Y. Zhang, Z.H. Wang, Y.Z. Zhang, Z.X. Zheng, C.M. Wang, Y.L. Du, W.C. Ye, Int. J. Electrochem. Sci. 7 (2012) 1968.
[39] X.J. Bian, X.F. Lu, E. Jin, L.R. Kong, W.J. Zhang, C. Wang, Talanta 81 (2010) 813.